Spectral Focal Sweep: Extended Depth of Field from Chromatic Aberrations

Oliver Cossairt
Columbia University
120th St, New York, NY 10027

ollie@cs.columbia.edu

Shree Nayar
Columbia University
120th St, New York, NY 10027

nayar@cs.columbia.edu

Abstract

In recent years, many new camera designs have been proposed which preserve image detail over a larger depth range than conventional cameras. These methods rely on either mechanical motion or a custom optical element placed in the pupil plane of a camera lens to create the desired point spread function (PSF). This work introduces a new Spectral Focal Sweep (SFS) camera which can be used to extend depth of field (DOF) when some information about the reflectance spectra of objects being imaged is known. Our core idea is to exploit the principle that for a lens without chromatic correction, the focal length varies with wavelength. We use a SFS camera to capture an image that effectively "sweeps" the focal plane continuously through a scene without the need for either mechanical motion or custom optical elements. We demonstrate that this approach simplifies lens design constraints, enabling an inexpensive implementation to be constructed with off-the-shelf components. We verify the effectiveness of our implementation and show several example images illustrating a significant increase in DOF over conventional cameras.

1. Introduction

Refractive materials such as glass and plastic bend light rays according to Snell's Law. According to this law, the bending power of a refractive surface is a function of the index of refraction (IOR) of the material. Because the IOR is in turn a function of wavelength, rays incident on a refractive surface are deflected different amounts according to their color. This phenomena is known as chromatic dispersion. In lens design, chromatic dispersion is considered undesirable because it results in lens aberrations which reduce image quality. However, chromatic aberrations produce a very useful property that can be exploited; a lens with axial chromatic aberrations has a focal length that varies as a function of wavelength. If such a lens is used with a black and white sensor, the imaging system can be thought of as possessing a continuum of focal lengths simultaneously. We call such a system a "Spectral Focal Sweep" (SFS) cam-

(a) An image captured with a corrected lens (8ms exposure)

(b) An image captured with a SFS camera (8ms exposure)

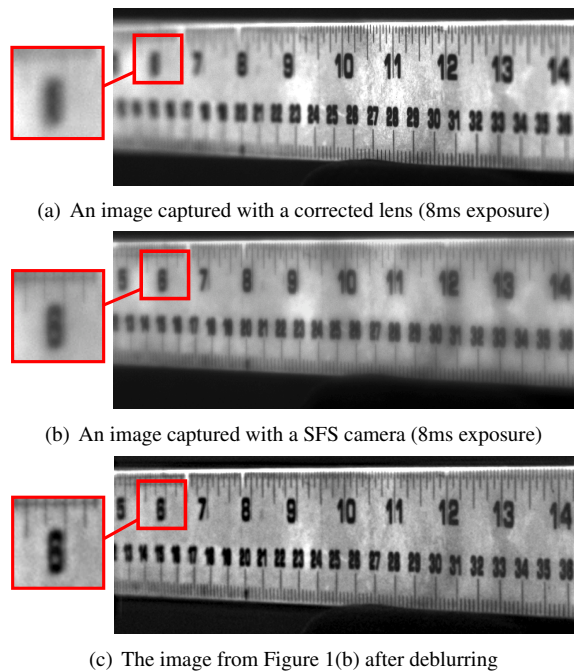(c) The image from Figure 1(b) after deblurring

Figure 1. Comparison of the SFS camera with a corrected lens. The image shown in Figure 1(a) was taken with a corrected lens. Images shown in Figures 1(b) and 1(c) were taken with a SFS camera. Figure 1(c) demonstrates that after deblurring, more detail is visible over a larger depth range when using the SFS camera.

era because it is analogous to existing focal sweep techniques [8][5] with one important distinction: it can be used to extend DOF with no moving parts.

For a SFS camera, the amount of focal sweep depends on the reflectance spectra of objects being imaged. The more broadband an object's spectrum, the wider the focal sweep. Thus, to function correctly, the camera requires objects being imaged to possess reasonably broad spectral reflectance distributions. Fortunately, the reflectance spectra of most real-world objects is sufficiently broadband [11]. We have observed that the SFS camera can effectively increase DOF for a wide variety of scenes (see Section 6, Figures 1, 8-11, and supplementary material). To further verify our claim that a SFS camera works effectively for most real-

Figure 2. A comparison showing the relative sizes and complexities of a Cosmicar 75mm F/1.4 lens (left) and our F/4 SFS doublet lens (right). Our lens is significantly lighter and more compact. The corrected lens is stopped down to F/4 in all experiments.
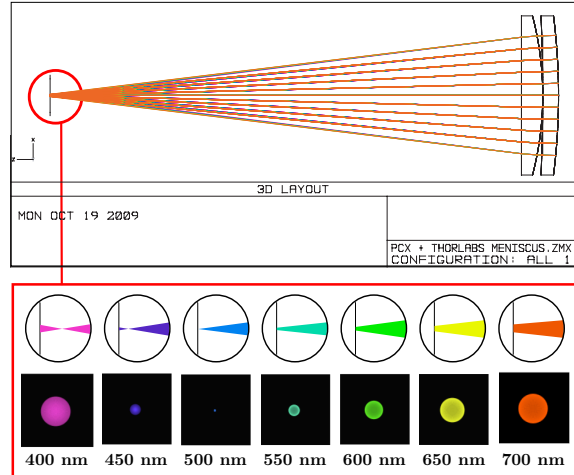

Figure 3. A SFS lens design is shown in the top figure. Below, a Zemax raytrace and PSF simulations are shown for various wavelengths. The lens exhibits strong axial chromatic aberration.

world spectra, we simulate the performance of our lens using the Munsell color database [9] in Section 5. The Munsell database consists of 1250 spectrophotometer readings of common reflectance spectra.

To design a SFS lens, we use an optimization that intentionally *maximizes* axial chromatic aberrations while minimizing other aberrations. This approach can greatly simplify lens design, reducing the cost and size of the design relative to a conventional lens design. We use this optimization to engineer a PSF which is not a delta function, but is approximately invariant to depth and preserves image details over a large depth range. We describe in detail the theoretical background for our work in Section 3.

We assume that depth in the scene being photographed varies over a large range, so that if a corrected lens is used, defocus blur removes important details (see Figure 1(a)). Our goal is to extend depth of field to preserve image details for all object distances in the scene (see Figure 1(c)). Furthermore, we wish to do so without sacrificing the signal-to-noise ratio (SNR) in our captured images. This rules out the option of increasing the F/# of our lens, which drastically decreases signal strength. Recently, significant attention has been paid to this problem, resulting in solutions that use either coded apertures [6][15], phase plates [2][7], or mechanical motion [8][5]. We discuss these and other related works in Section 2. While existing techniques *increase* complexity, our technique proposes to address the problem by *simplifying* the imaging system (see Figure 2). Rather than introducing new optical elements or mechanical motion, we reduce constraints on the camera lens, as described in Section 4, to achieve the same goal.

It is interesting to note that the SFS camera bears some similarity to NTSC and related video compression techniques. These techniques exploit the fact that the human visual system relies much more heavily on luminance information than color. Before compression is applied, images are first transformed to a different color space such as YUV or NTSC. After transformation, color channels in the image can be compressed more aggressively without significant perceptual degradation. The SFS camera can be thought to apply a similar compression to an image *before*

acquisition. For this reason, the SFS camera can be used to capture not only black and white images, but color images as well. To deblur color images, we use an approximate method that produces results which are not exact but *look good* (see Figures 10 and 11, and supplementary material).

2. Related Work

It has long been known that amplitude modulation of the pupil plane of a lens can increase DOF [14], a technique referred to as apodization. Since this discovery, several researchers have attempted to find optimal aperture patterns for extending DOF, including combinations of zone-plates as well as computer-generated amplitude holograms [10][12]. However, amplitude modulation reduces the optical efficiency of the lens, thereby reducing the signal strength relative to sensor noise.

Researchers have also developed camera systems which produce PSFs that are approximately depth invariant [1][2]. A notable example was introduced by Dowski et. al [2], who placed a cubic phase plate in the pupil plane of a camera system. They show analytically that such a camera produces a PSF that is approximately invariant to defocus. In addition, they argue that their PSF is more desirable than a conventional disc shaped defocus PSF because it preserves high frequencies and avoids zero crossings in the frequency domain. Techniques have also been introduced which produce a depth invariant PSF by sweeping either the sensor or object along the optical axis during exposure [8][5]. The PSFs for these techniques also preserve high frequencies since each object is instantaneously in focus at one point during exposure. However, they require the use of moving parts, which can be cumbersome and introduce limitations on the minimum exposure time.

Other works exist in the vision community which re-

	Type:Surf	Comment	Radius	Thickness	Glass	Semi-Diameter	Conic
1	Standard	LE1929	100.89	2.52	BK7	12.70	0
2	Standard		288.20	0.00		12.70	0
3	Even Asphere	48184	49.78	3.40	PMMA	12.70	-1
4	Even Asphere		0.00	75.23		12.70	0
	Polynomial Data		Parameter 0	Parameter 1	Parameter 2	Parameter 3	
3	Even Asphere		0	0	4.28E-07	2.83E-11	

Figure 4. The lens prescription data for the design shown in Figure 3.

cover an extended DOF image after first estimating scene depth [6][7][15]. The quality of these techniques, however, is closely coupled to the precision of depth estimation, since each region in the image is deblurred using an estimated defocus PSF.

The work most similar in spirit to the SFS technique is by DxO Optics [4], which also proposes to extend DOF by exploiting axial chromatic aberrations. This approach finds the color channel which is best focused and then transfers high frequency information from this channel to the remaining color channels. The scene details recovered using this technique are limited by the quality of the best focused channel. We show in the next section that for a system with axial chromatic aberrations, even the best focused color channel is blurred. This is because the spectra of real-world materials and the spectral response of color filters on the image sensor are broadband. Our SFS technique, on the other hand, can be considered analogous to existing focal sweep techniques. SFS imaging creates an approximately depth-invariant PSF. By deconvolving the captured image with the inverse of this PSF, an extended DOF image is recovered with details very close to what can be acquired with a corrected lens. In short, the SFS technique is able to recover more information (and hence DOF) than the frequency transfer method of DxO.

3. Theory

In this section, we describe the theoretical foundation for the SFS camera. We first consider the imaging properties of a 'thin' singlet (single element) refractive lens manufactured out of glass with IOR $n(\lambda)$, aperture diameter A, and radii of curvature R_1 and R_2, respectively. The focal length of this thin lens is [13]

$$f(\lambda) = (n(\lambda) - 1)\left(\frac{1}{R_1} + \frac{1}{R_2}\right). \qquad (1)$$

The dependence of focal length on wavelength is a result of the dispersive property of refractive materials, and this dependence, referred to as chromatic focal shift or axial chromatic aberration, is usually considered undesirable (see Figure 3). There are several well-established strategies for reducing its effect, e.g., by pairing two or more individual elements made from materials with complementary dispersive properties [3].

A singlet is usually insufficient for imaging onto a sensor because it exhibits strong spherical and field-dependent aberrations. To combat this, more elements are usually introduced to increase the degrees-of-freedom in the lens design optimization. The effective focal length $f_{EFL}(\lambda)$ of a compound lens can be calculated directly using the focal lengths and positions of individual elements. If a compound lens exhibits negligible spherical and field dependent aberrations, the irradiance $E(x, y, \lambda)$ of a point source with distance u from the lens and spectral reflectance $R(\lambda)$ can be written as

$$E(x, y, \lambda) = R(\lambda) \sqcap \left[\frac{r}{D(\lambda)}\right], \qquad (2)$$

where $r = \sqrt{x^2 + y^2}$, $\sqcap$ is the circ function:

$$\sqcap\left(\frac{r}{d}\right) = \begin{cases} \frac{1}{\pi d^2} & \text{if } r < \frac{d}{2} \\ 0 & \text{otherwise} \end{cases}, \qquad (3)$$

D is the chromatic defocus blur width which is determined from the gaussian lens law as

$$D(\lambda) = Av\left(\frac{1}{f_{EFL}(\lambda)} - \frac{1}{v} - \frac{1}{u}\right). \qquad (4)$$

Here, v is the sensor-to-lens distance, and A is the lens aperture diameter. A black and white sensor with spectral sensitivity $S(\lambda)$ will then measure a sampled version of the image irradiance $E(x, y)$ averaged over wavelength. If we assume that $S(\lambda)$ is constant with value $\frac{1}{\lambda_2 - \lambda_1}$ between wavelengths λ_1 and λ_2, and zero everywhere else, then we can write our PSF $P(x, y)$ as

$$P(x, y) = \int S(\lambda) E(x, y, \lambda) d\lambda \qquad (5)$$

$$= \frac{1}{\lambda_2 - \lambda_1} \int_{\lambda_2}^{\lambda_1} R(\lambda) \sqcap \left[\frac{r}{D(\lambda)}\right] d\lambda. \qquad (6)$$

Thus, the PSF for the SFS camera is a continuous sum of scaled concentric discs. We note that if $f_{EFL}(\lambda)$ varies linearly and the reflectance spectrum happens to be white, then the PSF is identical to the mechanical focal sweep PSF given in [8]. If, on the other hand, the reflectance spectrum is not white, then the sum is weighted by the magnitude of the spectrum for each wavelength.

4. Design and Implementation

The top of Figure 3 shows a raytrace of the doublet SFS lens design used in all the simulations and experiments in
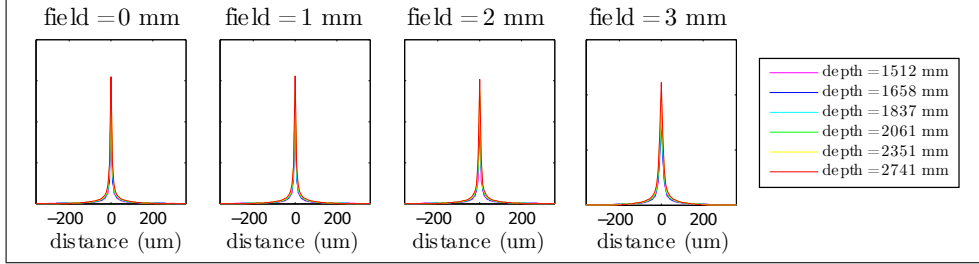
Figure 5. The simulated PSF for the lens in Figure 3 using a white spectrum. The PSF is shown as a function of depth and field position.

this paper. The lens was designed using Zemax Optical Design software. To optimize our lens, we maximized axial chromatic aberration over the wavelength range 400-700nm, while also minimizing PSF compactness for the center wavelength averaged over all field positions. We ran an optimization to create an F/4 75mm focal length lens consisting of two elements, which images onto a 1/3" sensor with 10μm pixel size. We found that a smaller spot size over a larger field of view can be achieved with a custom lens design. However, we decided to fit a design with off-the-shelf components from stock lens suppliers. The SFS lens design consists of an Edmund Optics plano-convex asphere (part #48184) and a Thorlabs positive meniscus (part #LE1929). The prescription is shown in Figure 4.

The bottom of Figure 3 shows the simulated PSF as a function of wavelength for our lens design. The wavelength-dependent PSF is shown to be the chromatic defocus disc given by Equation 2, where the disc diameter scales as a function of wavelength. The largest disc diameter, about 100μm, occurs at 400nm and 700nm. Because the focal length is not exactly a linear function of wavelength, the PSF with the smallest spot size is at 500nm, not the center wavelength of 550nm. Figure 5 shows the simulated PSF of our lens when using a black and white sensor with a white point source. The depth values were chosen so that the defocus blur size for the center wavelength is 100μm (the same as the maximum chromatic defocus) at the two extreme depths. Note that the PSF does not vary significantly with depth and field positions.

Figure 2 shows a side-by-side comparison of our SFS lens with a corrected Cosmicar lens, also designed for use with a 1/3" sensor. The relative complexities of the two designs are obvious from their relative sizes. While the Cosmicar lens is capable of imaging at a smaller F/#, it is significantly larger, heavier, and requires 5-6 elements as opposed to 2. The simplicity of our lens is a direct benefit of the SFS approach. Conventional lens designs minimize chromatic aberrations by adding a constraint to the lens optimization. Optimization with additional constraints requires more degrees of freedom, resulting in designs with the addition of more surfaces, and thus more elements. The SFS lens design does away with this costly constraint, allowing a reduction in complexity of the final design.

5. Design Verification

To verify our claim that our camera is useful for a wide variety of real-world scenes, we simulated the PSF for an assortment of reflectance spectra captured with a spectrophotometer. We downloaded the Munsell database of 1250 different recorded spectra and used Zemax to simulate the PSF of these spectra when imaged through our design. In our simulations, we used 50 wavelength samples to simulate the PSF $P_d(x,y)$ at $d = 1, 2, ...12$ depth locations. Again, the depth values were chosen so that the defocus blur size for the center wavelength is the same as the maximum chromatic defocus at the two extreme depths.

Figure 6 shows the results of our simulations. Figure 6(c) shows a cross section of the PSF for a few randomly selected spectra as a function of depth. Note that all of the PSFs have a strong peak, an indication that the PSFs preserve high frequencies. Also note that the PSF for each spectrum is relatively invariant to depth.

To quantitatively evaluate the quality of the PSFs from the Munsell database, we used the PSF distance measure $D(P_1(x,y), P_2(x,y))$ introduced by Zhou et. al [16]. This measure defines the similarity of two PSFs as the L2 norm of the Wiener reconstruction error for an image blurred by one PSF and then deconvolved with the other. For each Munsell color, we calculate the PSF distance for each $P_d(x,y)$ relative to the PSF at the center depth location. A plot of PSF distance is shown in Figure 6(a) for all Munsell colors, along with the PSF distance for a corrected lens (displayed as a dotted line). A flatter profile in this plot indicates less variation of the PSF with depth. The relative PSF distance for all Munsell colors imaged through the SFS lens is always less than for a corrected lens, significantly so for most colors. This indicates that the SFS lens always produces significantly more depth-invariant PSFs relative to a corrected lens.

To further evaluate the performance of our camera relative to existing extended-DOF designs, we computed the average PSF distance:

$$A = \frac{1}{12} \sum_{d=1}^{12} D(P_d(x,y), \tilde{P}_6(x,y)), \qquad (7)$$

where $\tilde{P}_6$ is the PSF of a white point source at the center depth. The quantity A measures the average reconstruction

(a) PSF variation   (b) Average PSF variation

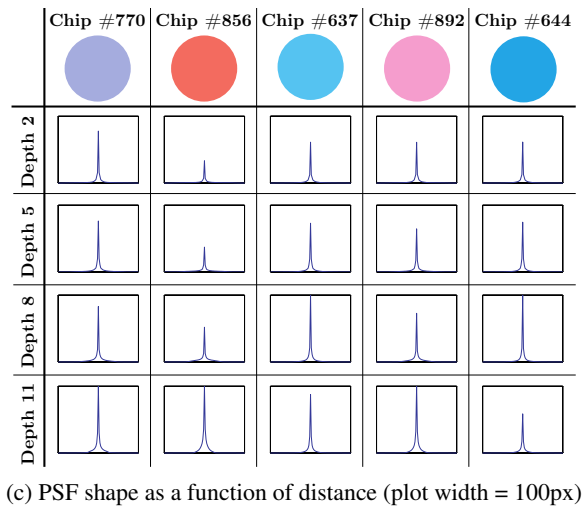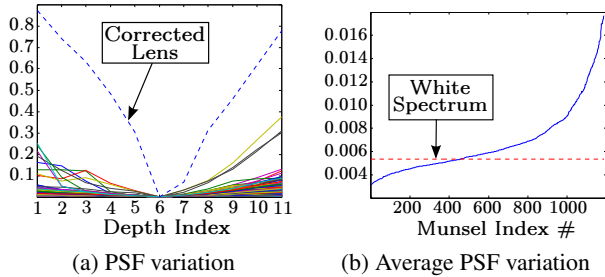(c) PSF shape as a function of distance (plot width = 100px)

Figure 6. Figure 6(a) shows PSF variation as a function of depth for all Munsell colors when imaged through the SFS lens. The dotted line denotes the PSF variation for all colors using a corrected lens. Note the flatness of all SFS profiles compared to the corrected lens, indicating that the PSF varies little with depth for most real-world colors. Figure 6(b) shows the average PSF variation for 95% of the Munsell dataset when imaged through the SFS camera. The dotted line denotes the average PSF variation for a white spectrum imaged through the SFS camera. Figure 6(c) shows that PSF shape is relatively invariant to depth for randomly selected Munsell colors. PSF height is normalized against the center PSF for each color.

error of a spectrum imaged by our SFS camera when a white spectrum is used for deblurring. To evaluate the deblurring quality of the Munsell colors, we compare the computed A value to that of a white spectrum. Figure 6(b) shows A for a large number of Munsell colors. As shown in the figure, for a white spectrum, $A \approx .005$. The Munsell colors are sorted in order of ascending A and the bottom 95% percent are shown. Notice that for 95% of the colors, $A \leq .02$. Thus 95% of the Munsell colors have a variation that is within a factor of 4 of a white spectra. This implies that most naturally occurring spectra will not introduce significant deblurring artifacts relative to a black and white scene.

For a corrected lens, $A \approx .5$, which is nearly two orders of magnitude greater than for a white spectrum image through our SFS camera. Figure 7 shows that the measured PSF of a white spectrum source imaged through our SFS

camera does indeed demonstrate significantly greater depth-invariance relative to a corrected lens.

6. Experiments

We now show several examples demonstrating the capabilities of our SFS lens. All black and white SFS images were captured using a Basler A311f VGA 1/3" sensor and the lenses shown in Figure 2. Color SFS images were captured using the same doublet SFS lens from Figure 2 and a Canon 450D sensor. Corrected lens examples were captured using a Cannon 100mm lens.

Deblurred images were generated using Wiener deconvolution with the PSF measured from a white point source (i.e. the bottom center PSF shown in Figure 7).

6.1. Black and White Images

Figure 1 shows a ruler captured by a F/4 corrected lens and our F/4 SFS lens after deblurring. The corrected lens image shows strong blurring in the front and rear of the ruler so that the numbers in the rear are barely legible. When the ruler is imaged by our camera, the numbers are legible over a larger depth range.

Figure 8 demonstrates that even for a scene with a variety of colors, image quality is superior to that achieved by stopping down a lens. Figure 8(a) shows a scene with plastic toys captured by a F/4 corrected lens. Details in the foreground and background are lost due to defocus blur. Figure 8(b) shows an image captured with the same exposure time but stopped down to F/16. The depth of field has been increased, but the SNR is greatly decreased due to weaker signal strength. Figure 8(c) shows an image captured with the F/4 SFS lens. Image details are clearly preserved over a larger depth range, but have a light haze due to the soft tail of the PSF. Figure 8(d) shows the results of deblurring Figure 8(c). The haze has been removed to improve contrast, resulting in crisp details over a larger depth range. The SNR is worse than in Figure 8(a), but significantly better than Figure 8(b).

Figure 9 shows an image of a resolution pattern at different depths to qualitatively present the level of detail that can be recovered with our technique. Notice that high frequency details which are completely lost in the corrected lens are clearly visible in the image taken with our camera.

6.2. Color Images

We have found that it is possible to use our SFS camera to restore color images using a simple and inexact approach that produces good visual results. We capture an RGB image with our SFS lens, then perform a YUV color transformation on the captured image. The resulting luminance channel closely approximates an image that would be captured with a black and white sensor. We deblur the luminance channel only, and transfer the image back to RGB

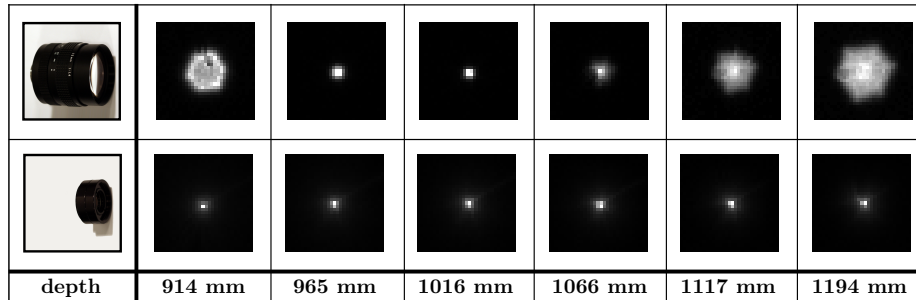| depth	914 mm	965 mm	1016 mm	1066 mm	1117 mm	1194 mm

Figure 7. The measured PSF using a white point source as a function of distance for both lenses shown in Figure 2 (The corrected lens is stopped down to F/4). For the corrected lens, the PSF shape is roughly a disc with diameter proportional to defocus. The SFS lens produces a PSF that is approximately depth invariant.

space. The method is inexact because it does not account for color bleeding in the chrominance channels. However, as discussed in the introduction, blurring in these channels is much less perceptible to humans, and we have found that the technique produces satisfactory results for a variety of scenes. Figures 10 and 11 show details of color reconstructions, demonstrating the fidelity of our inexact deblurring technique.

7. Limitations

While our technique does work well for a large variety of natural scenes, some naturally occurring spectra are not sufficiently broadband to produce a large spectral focus sweep range, and consequently produce a highly depth dependent PSF. The top 5% of Munsell colors (not shown) in Figure 6(b) have a PSF variation $V \geq .2$, some significantly larger. If our SFS lens is used to photograph a scene that contains narrowband reflectance spectra such as these, a significant amount of artifacts will be introduced after deblurring. Furthermore, while our approximate color deblurring method produces visually pleasing results, it does not correct for blurring in the chrominance channels, and is thus insuitable for many high quality imaging applications.

8. Conclusion

We have introduced a new lens design criterion that produces simpler designs and extends depth of field. In strong contrast to conventional lens design, our approach is to *maximize* chromatic aberrations, which are exploited for the purpose of extending depth of field. Our technique *reduces* lens complexity by relaxing constraints in the lens optimization process. While our technique does place some restrictions on the scene being imaged, we have shown that our design functions well for a wide variety of scenes. We implemented a SFS lens using off-the-shelf components, and presented a number of examples that demonstrate the effectiveness of our technique. Our implementation was shown to successfully increase depth of field for both black and white and color images.

References

[1] W. Chi and N. George. Electronic imaging using a logarithmic asphere. *Opt. Lett.*, 2001.

[2] J. E. R. Dowski and W. T. Cathey. Extended depth of field through wave-front coding. *Appl. Opt.*, 1995.

[3] J. M. Geary. *Introduction to Lens Design: With Practical Zemax Examples (Hardcover)*. Willmann-Bell, 2002.

[4] F. Guichard, H.-P. Nguyen, R. Tessières, M. Pyanet, I. Tarchouna, and F. Cao. Extended depth-of-field using sharpness transport across color channels. volume 7250. SPIE, 2009.

[5] G. Häusler. A method to increase the depth of focus by two step image processing. *Optics Comm.*, 1972.

[6] A. Levin, R. Fergus, F. Durand, and W. T. Freeman. Image and depth from a conventional camera with a coded aperture. In *SIGGRAPH '07*.

[7] A. Levin, S. Hasinoff, P. Green, F. Durand, and W. T. Freeman. 4d frequency analysis of computational cameras for depth of field extension. In *SIGGRAPH '09*.

[8] H. Nagahara, S. Kuthirummal, C. Zhou, and S. Nayar. Flexible Depth of Field Photography. In *ECCV '08*.

[9] U. of Joensuu Color Group. Spectral database. http://spectral.joensuu.fi/.

[10] J. Ojeda-Castaneda and L. R. Berriel-Valdos. Zone plate for arbitrarily high focal depth. *Appl. Opt.*, 1990.

[11] J. Parkkinen, J. Hallikainen, and T. Jaaskelainen. Characteristic spectra of munsell colors. *J. Opt. Soc. Am.*, 1989.

[12] J. Rosen and A. Yariv. Synthesis of an arbitrary axial field by computer-generated holograms. *Opt. Lett.*, 1994.

[13] W. J. Smith. *Modern optical engineering; the design of optical systems [by] Warren J. Smith*. McGraw-Hill, New York,, 1966.

[14] W. T. Welford. Use of annular apertures to increase focal depth. *J. Opt. Soc. Am.*, 1960.

[15] C. Zhou and S. Nayar. What are Good Apertures for Defocus Deblurring? In *ICCP '09*.

[16] C. Zhou and S. Nayar. Aperture evaluation for defocus deblurring and extended depth of field. *IEEE Trans. Pattern Analysis and Machine Intelligence (under review)*, 2010.

(a) Captured with a F/4 corrected lens (8ms exposure)

(b) Captured with our SFS lens (8ms exposure)

(c) Captured with a F/16 corrected lens (8ms exposure)
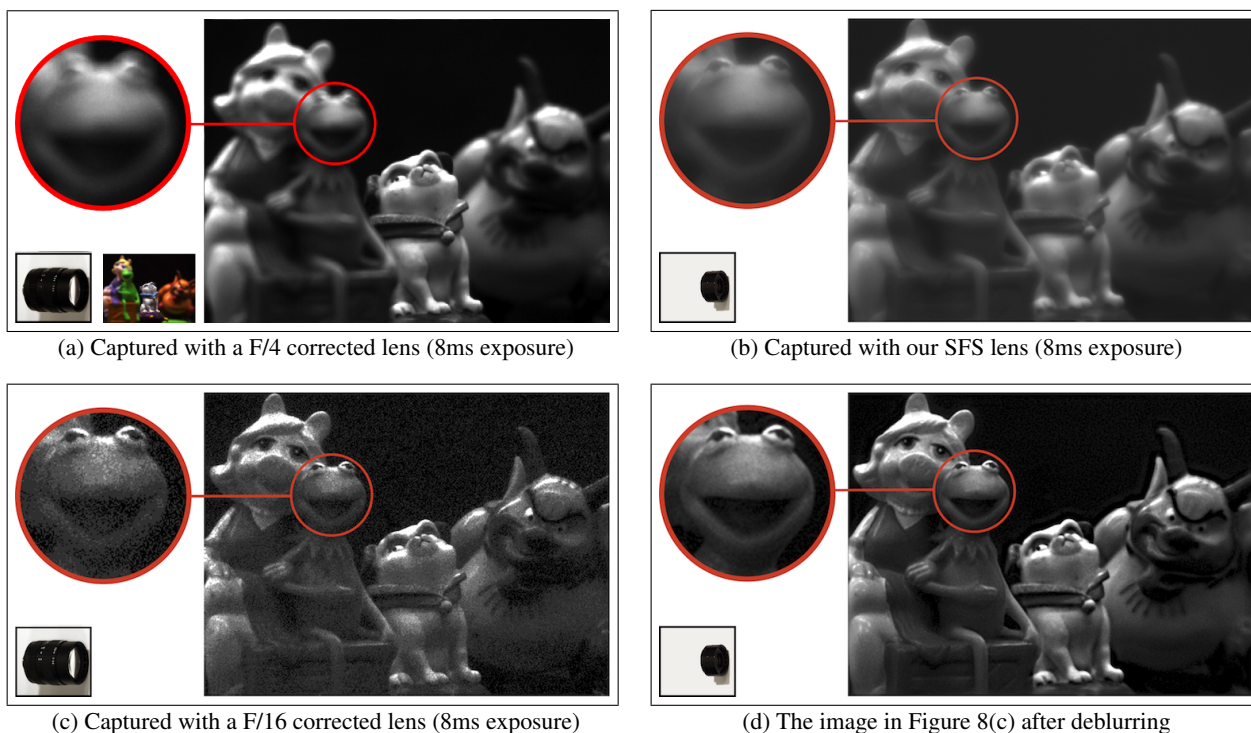
(d) The image in Figure 8(c) after deblurring

Figure 8. Comparison of the SFS camera with a corrected lens. All images are taken with an 8ms exposure time. Images on the left are taken with a corrected lens and images on the right are taken with our SFS camera. As shown in Figure 8(a), the DOF using a F/4 corrected lens is too narrow. Figure 8(c) shows that if we stop down to F/16 we achieve the desired DOF, but our image is corrupted by noise. When using our SFS camera, we capture the image in Figure 8(b), then recover the extended DOF image shown in Figure 8(d), which has significantly less noise. A color thumbnail is included in the bottom-left of Figure 8(a) to show the colors in the scene.

(a) An image captured with a F/4 corrected lens

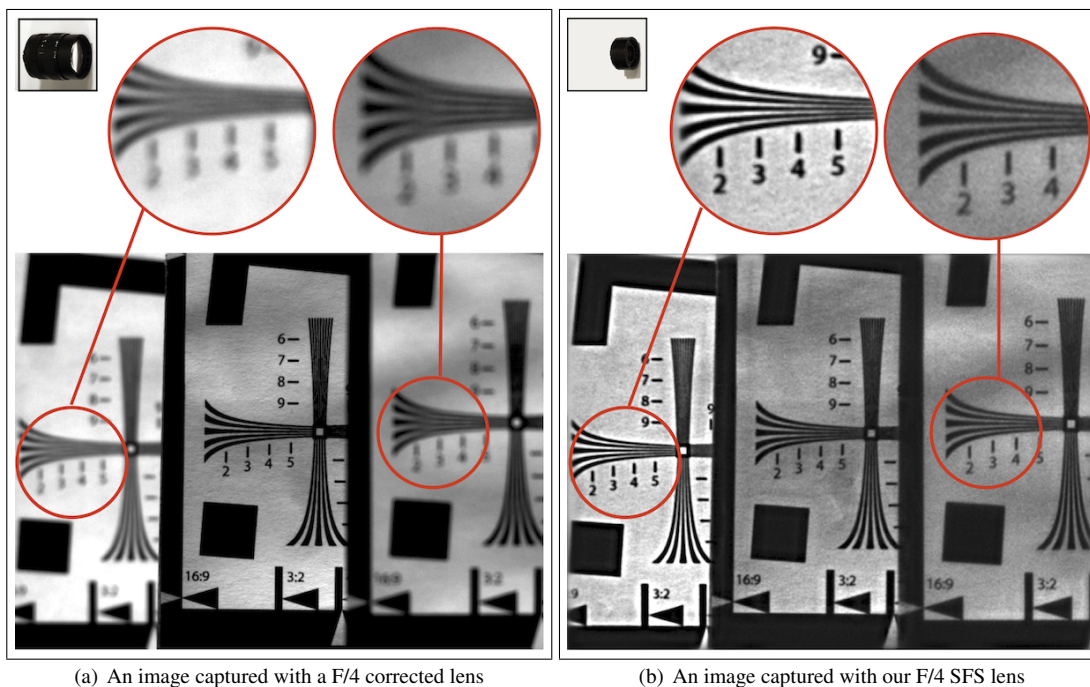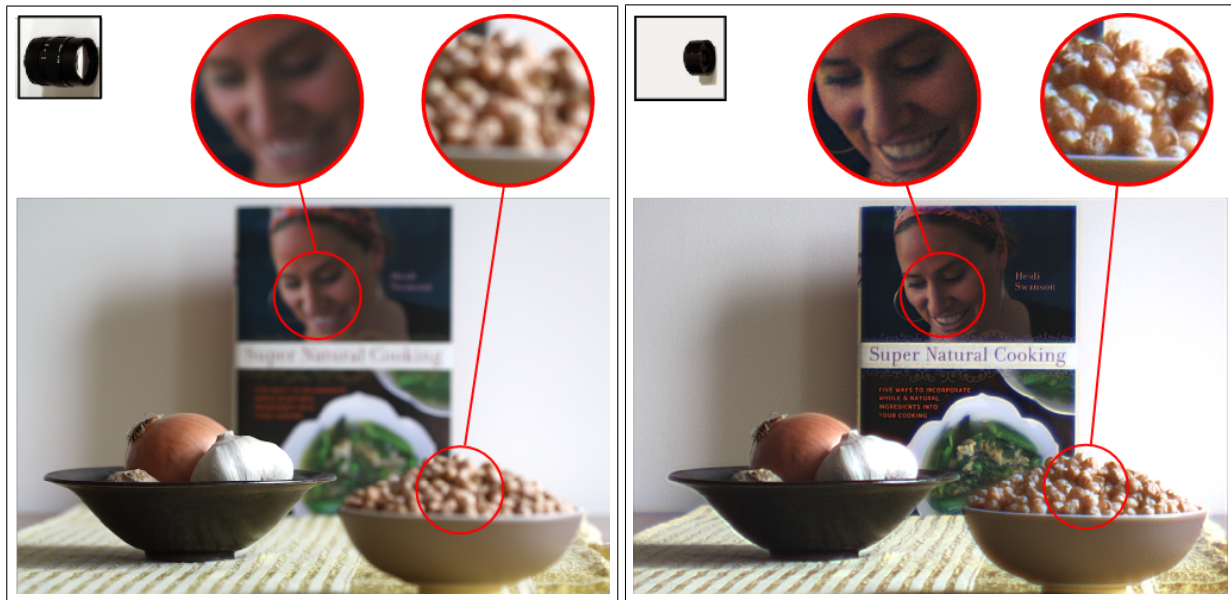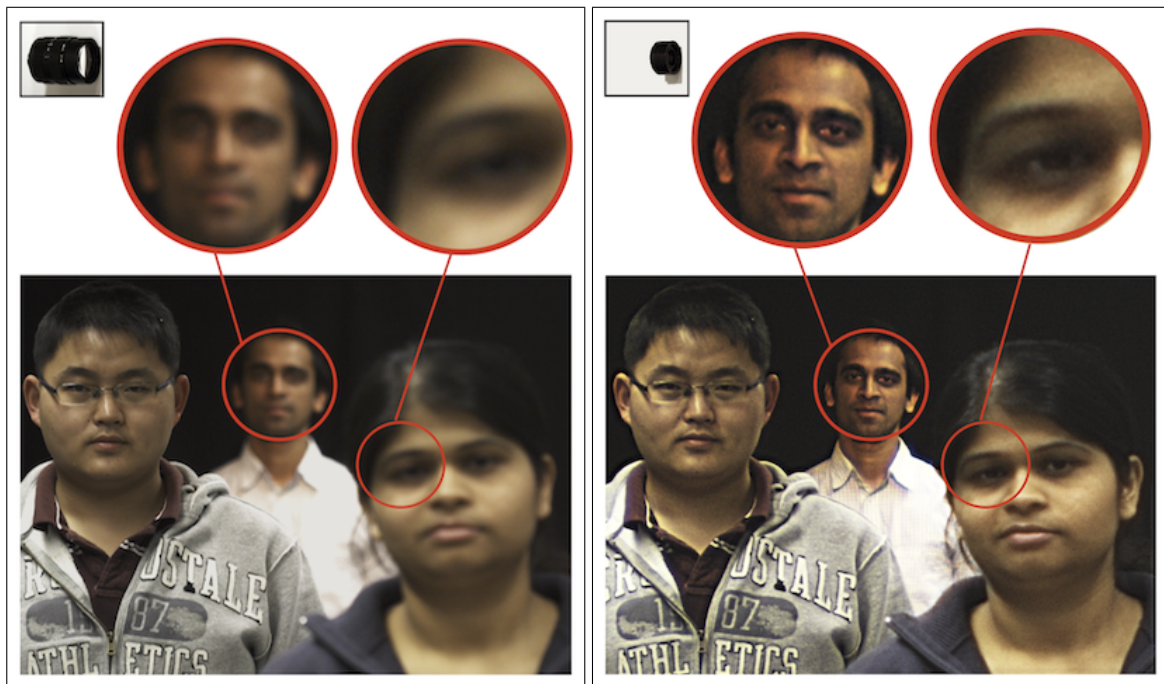(b) An image captured with our F/4 SFS lens

Figure 9. A scene consisting of three identical resolution targets placed at different depth planes. Images were captured with an 8ms exposure time and the corrected lens is stopped down to F/4. The left image was taken with a corrected lens, and the right image was taken with our SFS camera (after deblurring). The insets show that more detail is visible in the front and back planes when using the SFS camera.

(a) An image captured with a F/4 corrected lens   (b) An image captured with our F/4 SFS lens

Figure 10. A scene consisting of three objects placed at different depths on a table. Both images were taken with a 16ms exposure time and the corrected lens is stopped down to F/4. The image on the left was taken with a corrected lens and on the right is a deblurred version of an image taken with our SFS camera. The insets show that more detail is visible in the front and back objects when using our Spectral Focal Length camera.

(a) An image captured with an F/4 corrected lens   (b) An image captured with our F/4 SFS lens

Figure 11. A scene consisting of three people located at different depths. Both images were taken with a 16ms exposure time and the corrected lens is stopped down to F/4. The image on the left was taken with a corrected lens and on the right is a deblurred version of an image taken with our SFS camera. The insets show that more detail is visible in the front and back faces when using the SFS camera.